

The chemistry of fluorine-bearing molecules in diffuse and dense interstellar gas clouds

David A. Neufeld¹, Mark G. Wolfire², and Peter Schilke³

ABSTRACT

We present a theoretical investigation of the chemistry of fluorine-bearing molecules in diffuse and dense interstellar gas clouds, combining recent estimates for the rates of relevant chemical reactions with a self-consistent model for the physical and chemical conditions within gas clouds that are exposed to the interstellar ultraviolet radiation field. The chemistry of interstellar fluorine is qualitatively different from that of any other element, because – unlike the neutral atoms of any other element found in diffuse or dense molecular clouds – atomic fluorine undergoes an exothermic reaction with molecular hydrogen. Over a wide range of conditions attained within interstellar gas clouds, the product of that reaction – hydrogen fluoride – is predicted to be the dominant gas-phase reservoir of interstellar fluorine nuclei. Fluorine is the heavy element which shows the greatest tendency toward molecule formation; in diffuse clouds of small extinction, the predicted HF abundance can even exceed that of CO, even though the gas-phase fluorine abundance is four orders of magnitude smaller than that of carbon. Our model predicts HF column densities $\sim 10^{13} \text{ cm}^{-2}$ in dark clouds and column densities as large as 10^{11} cm^{-2} in diffuse interstellar gas clouds with total visual extinctions as small as 0.1 mag. Such diffuse clouds will be detectable by means of absorption line spectroscopy of the $J = 1 - 0$ transition at $243.2 \mu\text{m}$ using the Stratospheric Observatory for Infrared Astronomy (SOFIA) and the Herschel Space Observatory (HSO). The CF^+ ion is predicted to be the second most abundant fluorine-bearing molecule, with typical column densities a factor $\sim 10^2$ below those of HF; with its lowest two rotational transitions in the millimeter-wave spectral region, CF^+ may be detectable from ground-based observatories. HF absorption in quasar spectra is a potential probe of molecular gas

¹Department of Physics and Astronomy, Johns Hopkins University, 3400 North Charles Street, Baltimore, MD 21218; neufeld@pha.jhu.edu

²Department of Astronomy, University of Maryland, College Park, MD 20742; mwolfire@astro.umd.edu

³Max-Planck-Institut für Radioastronomie, Auf dem Hügel 69, 53121 Bonn, Germany; schilke@mpifr-bonn.mpg.de

at high redshift, providing a possible bridge between the UV/optical observations capable of probing H_2 in low column density systems and the radio/millimeter-wavelength observations that probe intervening molecular clouds of high extinction and large molecular fraction; at redshifts beyond ~ 0.3 , HF is potentially detectable from ground-based submillimeter observatories in several atmospheric transmission windows.

Subject headings: ISM: Molecules — ISM: Abundances — ISM: Clouds – molecular processes – infrared: ISM – submillimeter

1. Introduction

To date, molecules containing the ten elements hydrogen, carbon, nitrogen, oxygen, fluorine, silicon, phosphorus, sulfur, chlorine, and iron have been detected in the interstellar medium (ISM).¹ While the chemical processes leading to the formation and destruction of molecules containing the more abundant of these elements (e.g. H, C, N, O, Si, S) have been the subject of extensive theoretical investigation over a period of several decades, the chemistries of the less abundant elements have received far less attention. In particular, no systematic theoretical study of the chemistry of interstellar fluorine-bearing molecules has yet been undertaken, although a preliminary investigation undertaken following the discovery of interstellar hydrogen fluoride (Neufeld et al. 1997; hereafter NZSP) suggested a strong tendency towards the formation of HF; this investigation suggested that HF would be the overwhelmingly dominant reservoir of gas-phase F nuclei over a wide range of physical conditions, and led NZSP to argue that observations of HF provided a particularly useful probe of the depletion of interstellar molecules onto icy grain mantles within cold, shielded regions of the ISM.

In this paper, we report the first systematic study of the chemistry of interstellar fluorine. This study is motivated by several recent and current developments: (1) the discovery of interstellar hydrogen fluoride in 1997 (NZPS); (2) new quantal calculations of the rate coefficient for $\text{F} + \text{H}_2 \rightarrow \text{H} + \text{HF}$ (Zhu et al. 2002), which strengthen further the case for large HF abundances over a wide range of interstellar conditions; (3) the prospects for the widespread detection of HF absorption with upcoming airborne and satellite submillimeter telescopes; (4) the potential utility of HF observations as a probe of the depletion of interstellar molecules onto icy grain mantles.

¹In addition, the molecules containing the elements Na, Mg, Al, and K have been detected in circumstellar outflows.

In §2, we present a discussion of the fundamental chemical and photochemical processes leading to the formation and destruction of fluorine-bearing molecules in interstellar gas clouds. In §3, we discuss a model for the chemistry of fluorine in diffuse and dark clouds irradiated from the outside by ultraviolet radiation. Predicted abundances and column densities of fluorine-bearing species are presented for a range of physical parameters relevant to the interstellar medium. A discussion of these results follows in §4, with particular emphasis on the prospects for future observations.

2. Interstellar fluorine chemistry

2.1. Overview: thermochemistry of F-bearing species

The large dissociation energy of hydrogen fluoride makes the chemistry of interstellar fluorine qualitatively different from that of any other element. This key feature of the fluorine chemistry is made clear in Table 1, which lists the standard heats of formation of the hydrides and fluorides of the elements C, N, O, Si and S. The values presented here are relative to the enthalpies of formation of the constituent atoms; the tabulated quantity is therefore $\Delta_f H_{\text{gas}}^0(\text{XY}) - \Delta_f H_{\text{gas}}^0(\text{X}) - \Delta_f H_{\text{gas}}^0(\text{Y})$. In each case, the enthalpies recommended by the NIST Chemistry Web book² were adopted. The values presented for molecular ions make use of the ionization potentials recommended by the NIST Chemistry Web book, and any differences between the specific heat capacity of each ion and its corresponding neutral were neglected.

The thermochemical data presented in Table 1 show that atomic fluorine – unlike C, C⁺, N, O, Si, Si⁺, S or S⁺ – can undergo exothermic reaction with H₂ to form a diatomic hydride. Thus, the reaction of the dominant ionization state of fluorine (F) with the dominant molecular constituent of the interstellar gas (H₂) potentially provides a uniquely efficient pathway to the formation of HF. The chemistry of interstellar chlorine shows some similarity to that of fluorine, in that Cl⁺, the dominant ionization state of chlorine in atomic clouds, reacts exothermically with H₂ to form HCl⁺. A critical difference between the two cases, however, is that HCl⁺ – unlike HF of course – undergoes dissociative recombination to produce Cl. Thus atomic chlorine, which does not react exothermically with H₂, is predicted to become the dominant ionization stage at precisely the point at which the molecular fraction becomes large.

²NIST Standard Reference Database Number 69, Eds. P. J. Linstrom and W. G. Mallard, March 2003, National Institute of Standards and Technology, Gaithersburg MD, 20899; available on-line at <http://webbook.nist.gov>

A second implication of the data presented in Table 1 is that HF – once formed – is not easily destroyed. Reactions with C, N, O, Si, S and S⁺ are all substantially endothermic and therefore negligibly slow at the low temperatures that characterize molecular clouds. Table 2 presents the heats of reaction for 20 possible reactions that might destroy HF. Of these, only reactions with C⁺, CH, CH⁺, Si⁺, SiH, and SiH⁺ are exothermic³. Given the typical temperatures and chemical composition in molecular clouds, the reactions of HF with C⁺ and Si⁺ are expected to be the most important of the those listed in Table 2, leading to the stable molecular ions CF⁺ and SiF⁺ that are isoelectronic with CO.

In Table 3, proton affinities are compared for several astrophysically important molecules. Here again, rather few proton transfer reactions that could destroy HF can proceed exothermically: at the low temperatures in molecular clouds, only H₃⁺ and H₂⁺ can react with HF to form H₂F⁺. Furthermore, the ionization energy of HF (16.03 eV) being larger than that of H, HF does not undergo exothermic charge transfer with H⁺ and – like atomic fluorine – cannot be photoionized by radiation longward of the Lyman limit.

In the remainder of this section, we present a detailed discussion of the primary formation and destruction mechanisms for hydrogen fluoride.

2.2. Formation of HF

The reaction



has been the subject of intensive experimental and observational study, the results of which have been reviewed recently – and added to – by Zhu et al. (2002). The reaction has an activation energy barrier $\sim 4 \text{ kJ mol}^{-1}$, although the reaction rate is significantly enhanced at low temperatures by tunneling and is finite at zero temperature (Balakrishnan & Dalgarno 2001). Thus, at the temperatures $T \sim 10 - 100 \text{ K}$ typical of molecular clouds, the rate coefficient was substantially underestimated by the simple Arrhenius expression that we adopted in NZSP to extrapolate from laboratory measurements obtained at higher temperatures. Here instead, we adopt the results of the detailed calculations obtained by Zhu et al. (2002) and kindly made available to us for temperatures (10 – 50 K) outside the range computed previously. At the densities typical of the interstellar medium, atomic fluorine is found primarily in the ground $^2P_{3/2}$ fine-structure state (Zhu et al. 2002), which has a higher rate coefficient than $^2P_{1/2}$ for reaction with H₂. The overall rate of reaction of H₂ with F is

³In NZSP, we erroneously included Si⁺ in the list of species that cannot react exothermically with HF

therefore well-approximated by the specific rate for reaction with F ($^2P_{3/2}$). Figure 1 shows the rate coefficients computed by Zhu et al. for the reaction of F ($^2P_{3/2}$) with H₂ $J = 0$ (red crosses) and $J = 1$ (blue crosses). Black crosses show a weighted average applicable when the H₂ populations are in local thermodynamic equilibrium (LTE)⁴, and the solid black curve shows our adopted fit to that average (see Table 4), which is accurate to better than 5% throughout the temperature range plotted.

Some remaining uncertainty is associated with the F + H₂ potential energy surface (PES). As Zhu et al. and others have noted, a more recent PES that has been computed with account taken of the spin-orbit interaction (Castillo et al. 1998; hereafter the HSW potential) appears to yield a *poorer* fit to the experimental data than an earlier PES for which the spin-orbit interaction was neglected (Stark & Werner 1996; hereafter SW). In particular, the barrier in the HSW potential appears to be too high. Accordingly, Zhu et al. adopted the earlier SW PES in the calculations that they presented.

In NZSP, we argued that the reaction of F with H₂O might provide an important additional HF formation route at low temperatures ($T \leq 30$ K) for which the F + H₂ reaction rate was small. The rate coefficient for the reaction



has been measured by Stevens et al. (1989) as $(1.6 \pm 0.3) \times 10^{-11} \text{cm}^3 \text{s}^{-1}$. The rate coefficient showed no detectable variation over the temperature range 240–373 K and the implied limit on any activation energy barrier was (-28 ± 42) K. Here, we adopt the same rate coefficient. The importance of reaction (R2), however, is diminished because the adopted rate coefficient for (R1) is now much larger than what we previously assumed in the low temperature regime.

2.3. Destruction of HF

2.3.1. Ion-neutral reactions

As discussed in §2.1 above, HF can react exothermically with the ions C⁺, Si⁺ and H₃⁺ in the reactions



⁴The exact ortho-to-para ratio for H₂ has been the subject of considerable theoretical and observational study. In the diffuse molecular clouds, the observed ratio H₂ $J = 1$ / H₂ $J = 0$ is generally consistent with LTE (e.g. Savage et al. 1977), although the value in dark clouds is less well constrained. Fortunately, in this case, the reaction rates for H₂ $J = 1$ and H₂ $J = 0$ are not that dissimilar.



In addition, dissociative charge transfer with He^+ is also exothermic:



For molecules with large dipole moments such as HF, the rates of ion-neutral reactions are expected (e.g. Adams, Smith & Clary, 1985) – and indeed observed (e.g. Rowe et al. 1985) – to increase significantly with decreasing temperature. To our knowledge, none of the reactions (R3)–(R6) has been measured at interstellar temperatures. In estimating the rate coefficients for these reactions, we have made use of the statistical adiabatic capture model (SACM; Troe 1985, 1987, 1996) to determine the rate of ion-dipole capture, together with the assumption that the reaction probability following capture is unity. In this approximation, the capture rate depends solely upon the dipole moment, $\mu_D = 1.826$ Debye; the polarizability, $\alpha = 2.4 \times 10^{-24} \text{ cm}^3$; the rotational constant, $B = 20.54 \text{ cm}^{-1}$; and the reduced mass of the reacting system, μ .

The capture rate is given in the limit of low temperature ($T \lesssim hcB/k$), by the expression

$$k_a = k_L(1 + \mu_D^2/3\alpha hcB)^{1/2}, \quad (1)$$

where $k_L = 2\pi|q|(\alpha/\mu)^{1/2} = 3.6 \times 10^{-9} \text{ cm}^3\text{s}^{-1}$ is the Langevin rate coefficient for reactions involving an ion of charge q (i.e. the value that would obtain in the absence of any permanent dipole moment.) Gaussian electrostatic units are adopted here, with α having dimensions of length³ and μ_D having units of e.s.u. \times length. At temperatures $T \gtrsim hcB/k$, the reaction rate can be approximated by

$$k_b = k_L(1 + f\mu_D(2/\pi\alpha kT)^{1/2}) \quad (2)$$

(Troe 1987; using the simplified analytic expressions in the Appendix), where $f \sim 0.4$ if the HF rotational states are thermally-populated and $f \sim 1$ if HF is rotationally cold. (This high-temperature case is often referred to as the average dipole orientation (ADO) approximation and the specific case $f = 1$ as the locked-dipole approximation.) The low and high temperature regimes are bridged by the expression

$$k_{cap} = k_b [1 - \exp(-k_a/k_b)] \quad (3)$$

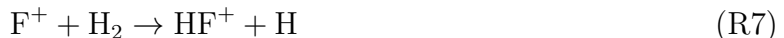
Using this model, we computed the rate coefficients for reactions (R3) – (R6) over the temperature range 10 to 100 K and then fit a power-law to the temperature dependence.

Because interstellar densities are typically much smaller than the critical density⁵ at which the HF $J = 1$ rotational state reaches its LTE population, we considered the case where HF is rotationally-cold (i.e. entirely in the ground state, $J = 0$.) The result of the power-law fit was

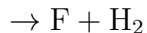
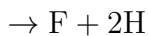
$$k_{cap} = 2.0 \times 10^{-8} (T/300\text{K})^{-0.15} (\mu/\text{a.m.u.})^{-1/2} \text{cm}^3 \text{s}^{-1} \quad (4)$$

and maximum error in the power-law fit was 12% over the temperature range 10 – 100 K.

Fluorine ions produced in reaction (R6) can undergo a series of two exothermic hydrogen atom abstraction reactions to form H_2F^+ :



We adopt the estimates (see Table 4) provided by Le Teuff, Millar & Markwick (2000; a.k.a. the UMIST ratefile) for the rate coefficients of the analogous reactions involving the element chlorine. The exact value of these rate coefficients has no bearing upon the overall HF abundance because every F^+ ion produced by reaction (R6) is rapidly converted to H_2F^+ . Reaction of CF^+ with H_2 to form HCF^+ is endothermic by 180 kJ mol⁻¹ and is therefore negligibly slow at the temperatures of interest. The molecular ions produced by reactions (R3) – (R8) are destroyed by dissociative recombination (DR) via the reactions



We are unaware of any experimental or theoretical studies that specifically address the rates of these reactions. We therefore adopt a rate coefficient typical of other DR reactions: $2 \times 10^{-7} (T/300)^{-1/2} \text{cm}^3 \text{s}^{-1}$ for diatomic ions [(R9) – R(11)] and $7 \times 10^{-7} (T/300)^{-1/2} \text{cm}^3 \text{s}^{-1}$ for polyatomic ions [reaction (R12)]. The exact value adopted does not affect the predicted HF abundance (although, of course the minor species CF^+ , SiF^+ , and H_2F^+ will have abundances that vary inversely with their assumed DR rate coefficients). The branching ratio

⁵The critical density at which the rate of collisional de-excitation equals the spontaneous radiative decay rate is $n(\text{H}_2) \sim 10^{10} \text{cm}^{-3}$ at 50 K, given the collisional rate coefficients computed by Reese et al. (2005)

for the DR of H_2F^+ will affect the effective rate of HF destruction via reactions (R5) and (R6), because HF is immediately reformed unless DR leads to atomic fluorine. We assume a branching ratio of one-half for the formation of atomic fluorine.

2.3.2. Photodissociation of HF

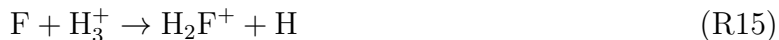
The photoabsorption spectrum of HF (Hitchcock et al. 1984; Nee, Suto & Lee 1985), together with theoretical potential energy curves (e.g. Brown & Balint-Kurti 2000; see Figure 2) imply that photodissociation is dominated by absorption to the repulsive $\text{A}^1\Pi$ state, which has a vertical excitation energy $\sim 84000 \text{ cm}^{-1}$. Theoretical calculations (Brown & Balint-Kurti 2000) indicate a maximum photodissociation cross-section of $3.25 \times 10^{-18} \text{ cm}^2$ for HF at a wavelength of 119 nm, values in good agreement with the experimental results of Nee, Suto & Lee (1985). The maximum cross-section must still be regarded as somewhat uncertain, however, because experimental results of Hitchcock et al. (1984) suggest a value that is larger by a factor 2.

Given the photodissociation cross-section given by Brown & Balint-Kurti, we obtained a HF photodissociation rate of $1.17 \times 10^{-10} \text{ s}^{-1} \chi_{UV}$, where χ_{UV} is the mean intensity of the radiation field normalized with respect to the standard interstellar ultraviolet (ISUV) radiation field of Draine (1978). For the case of a semi-infinite slab that is illuminated isotropically, we determined how the HF photodissociation rate varies with position using photodissociation region model of Le Bourlot et al. (1993), which provides as output the UV radiation field as a function of depth into an interstellar cloud. We found that the photodissociation rate diminishes as $E_2(2.21A_V)$, where A_V is the visual extinction in magnitudes behind the slab surface and E_2 is the exponential integral of order 2. The UV dust albedo assumed here was $\omega = 0.32$ and the forward scattering function was 0.73 (Li & Draine 2001).

In the deep interiors of clouds with substantial A_V , the UV radiation field is dominated by Lyman and Werner band emissions from H_2 molecules that have been excited by the secondary electrons ejected by cosmic rays (e.g. Prasad & Tarafdar 1983). The resulting photodissociation rates have been presented for several molecules of astrophysical interest by Sternberg, Dalgarno & Lepp (1987; hereafter SDL87) and by Gredel et al. (1989). We have computed the rate of cosmic-ray induced photodissociation for HF, adopting similar methods to those described by Gredel et al. (1989). Here we used the H_2 UV spectrum plotted in SDL87 (Figure 1) with the more recent excitation yields given by Dalgarno, Yan & Liu (1999; Table 2). The result is $87 \zeta_{\text{cr}}/(1-\omega)$, where ζ_{cr} is the total cosmic ray ionization rate per H_2 molecule.

2.4. Other reactions

Although we do not expect them to be significant, for completeness we include the following additional reactions in the chemical network leading to HF:



For reactions (R13) and (R14), we adopt the same rate coefficient assumed for reaction (R2). As in the case of nitrogen, proton transfer from H_3^+ to F is endothermic, but reaction (R15) is exothermic. Here we adopt the rate coefficient measured for the analogous reaction with N (Scott et al. 1997).

The rate coefficients for reactions for the entire fluorine reaction network (R1) – (R15) are summarized in Table 4, together with the rates of photodissociation by the interstellar and cosmic-ray-induced UV radiation fields.

3. Interstellar cloud model

We have used a modified version of the photodissociation region (PDR) models of Kaufman et al. (1999; hereafter K99), Wolfire et al. (1990), and Tielens & Hollenbach (1985) to examine the chemistry of fluorine molecules in diffuse and dense molecular clouds. In §3.1 we discuss results for a cloud model illuminated from one side and in §3.3 we discuss results for a cloud model illuminated from two sides. The PDR models solve simultaneously for the thermal balance and chemical equilibrium abundances of a layer of gas illuminated by a far-ultraviolet ($6 \text{ eV} \leq h\nu \leq 13.6 \text{ eV}$; FUV) radiation field.⁶

The PDR model for 2-sided illumination is based on the one-sided illumination models but modified so as to allow for illumination from both sides. In the one-sided case, calculation of the chemistry, cooling, and line-transfer proceeds from the surface to the cloud center

⁶In the K99 models the radiation intensity incident on the cloud was normalized to units of the Habing (1968) field. Here, we adopt a Draine (1978) field which has an integrated 6 eV to 13.6 eV intensity that is 1.7 times higher than Habing and denote this field strength as $\chi_{UV} = 1$. Although Weingartner & Draine (2001) have recently advocated using the field derived by Mezger et al. (1982) and Mathis et al. (1983) (1.13 times Habing), Parravano et al. (2003) found a median field closer to that of Draine (1978). Furthermore, Wolfire et al. (2003) found that a field 1.7 times Habing provides a good match to the temperature and pressure of the cold and warm phases of the local ISM.

in a single pass since these parameters depend only on the cloud properties closer to the surface. In the two-sided case, since shielding and cooling may be important toward both sides of the cloud, an iterative procedure is required. We first calculate the structure of a cloud illuminated from one side to a depth of one-half the visual extinction of the desired two-sided model. This provides us with initial estimates of line optical depths as well as shielding columns of H_2 and CO . In the two-sided model, a particular point in the cloud sees FUV radiation from both sides and cooling radiation may escape toward either surface; thus we iterate the chemical profiles, optical depths, and shielding factors.

Modifications to the physics and chemistry assumed in the K99 model have been discussed in Wolfire et al. (2003), who assumed a higher abundance of PAHs and a slower rate of interaction of ions and PAHs. These changes largely offset each other with a resulting minor effect on the grain heating rates and ion chemistry. In addition, we have adopted the results of Péquignot (1990) for the rate coefficient for collisional excitation of O I by H, and those of McCall et al. (2003) for the H_3^+ dissociative recombination rate coefficient.

For the case of the one-sided cloud models, we have implemented an additional modification by using a subroutine based upon the publically-available⁷ code from the Meudon group (Le Bourlot et al. 1993; Le Petit et al. 2002) to treat H_2 dissociation, H_2 heating and H_2 cooling, although we retain the H_2 formation rate of $3 \times 10^{-17} n_{\text{H}} n(\text{H}) \text{ cm}^{-3} \text{ s}^{-1}$ adopted in K99. Additional details of our method, test cases, and results, are discussed in (Kaufman et al. 2005).

3.1. One-sided illumination

We first consider the case of a constant-density slab that is illuminated from one side by ultraviolet radiation. As our standard model for a diffuse cloud, we adopt a density of H nuclei $n_{\text{H}} = 10^2$, and a radiation field equal to the average interstellar value given by Draine (1978), $\chi_{UV} = 1$. The illumination is assumed to be isotropic within the hemisphere incident upon the slab surface.

In Figure 2, we show the temperature profile and molecular abundances plotted as a function of the depth into the cloud (measured in units of visual extinction, A_V). Here, we assume a constant gas-phase fluorine abundance of 1.8×10^{-8} relative to H nuclei. The adopted value is chosen to fit the abundances $\text{F}/\text{O} = (3.8 \pm 1.7) \times 10^{-5}$ and $\text{O}/\text{H} = (4.2 \pm 0.2) \times$

⁷<http://aristote.obspm.fr/MIS/>

10^{-4} derived by Federman et al. (2005) from FUSE observations of atomic fluorine⁸ along the sightline to HD 208440. Similar F/O abundances were inferred from FUSE observations of FI in HD 209339A and from the original discovery of FI toward δ Sco (by *Copernicus*; Snow & York 1981). The assumed gas-phase fluorine abundance corresponds to roughly $0.6 \times$ the solar abundance of fluorine. The possible effects of fluorine depletion in dense regions are considered in §3.4 below.

The strong tendency towards HF formation is immediately apparent from Figure 2: HF accounts for at least 50% of the gas-phase fluorine nuclei at all depths $A_V \gtrsim 0.1$. Figure 3 compares the rates of various HF formation and destruction processes as a function of depth into the cloud. At all A_V , HF formation is dominated by reaction of F with H_2 (reaction R1). At small A_V ($A_V \lesssim 2$ for this particular case), HF destruction is dominated by reaction with C^+ (R3) and by photodissociation by ISUV radiation. These processes become less rapid with increasing A_V as the C^+ abundance drops in favor of C and CO and the ISUV field is attenuated by dust absorption. For intermediate A_V (in the range $\sim 2 - 4$ for this case), reaction with Si^+ (R4) becomes dominant. Once the Si^+ density begins to drop at $A_V \gtrsim 4$, HF destruction is dominated by reaction with H_3^+ and He^+ . In this regime, the abundances of H_3^+ and He^+ are controlled by the cosmic ray ionization rate and are essentially independent of A_V ; this effect provides a “floor” below which the total HF destruction rate never drops.

3.2. Parameter study

We also obtained results for incident radiation with intensities, χ_{UV} , of 10^{-1} , 1, 10, 100, 10^3 , and 10^4 times the average radiation field given by Draine (1978); and for H nucleus densities, n_H , of $10^{1.5}$, 10^2 , $10^{2.5}$, 10^3 , $10^{3.5}$, and 10^4 cm^{-3} . In Figure 4, we present HF abundance profiles for selected cases covering a wide range of assumed density and ISUV field. Here the abundance plotted is normalized with respect the total gas-phase abundance of fluorine nuclei. The tendency to HF formation is strikingly robust. In every case we considered, substantial HF abundances are achieved at depths $A_V > 2$ below the cloud surface. Indeed, the abundance of HF closely mirrors that of H_2 (as expected given the fact that HF is formed by direct reaction of H_2 with F). Figure 5 shows the same data presented in Figure 4, now expressed in terms of HF/ H_2 abundance ratio; its value always lies within an order of magnitude of 3.6×10^{-8} , the value achieved in the limit of large A_V when H_2 and HF are the dominant reservoirs of gas-phase H and F nuclei.

⁸Due to the formation of HF, the assumed gas-phase fluorine abundance in our model is $\sim 15\%$ higher than the predicted FI abundance for a cloud with properties appropriate to the HD 208440 sightline.

3.3. Two-sided illumination

We have extended the results presented in Figures 4 and 5 to the case where radiation is incident upon both sides of slab of finite thickness. Here calculations made use of the modifications to the PDR code described at the beginning of §3. In Figure 6, solid lines show the total H₂ and HF column densities, $N(\text{H}_2)$ and $N(\text{HF})$, in a slab with $\chi_{UV} = 1$, $n_{\text{H}} = 10^2 \text{cm}^{-3}$; the results are shown as a function of the total visual extinction through the cloud, $A_V(\text{tot})$. As expected from Figure 5, the H₂ and HF column densities track each other closely. In Figure 7, we plot $N(\text{HF})$ as a function of $N(\text{H}_2)$ for several values of χ_{UV} and of n_{H} . The dashed line corresponds to $N(\text{HF})/N(\text{H}_2) = 3.6 \times 10^{-8}$, the value obtained in the limit where H₂ and HF are the sole gas-phase reservoirs of H and F nuclei. In Figure 8, $N(\text{HF})$ is shown as a function of $A_V(\text{tot})$.

We note that the column densities and visual extinctions plotted in Figures 6 – 8 all refer to a single slab viewed face-on. Geometric effects can lead to significant multiplicative factors that affect the measured column densities and extinctions. For example, a plane-parallel slab viewed at an inclination angle θ will show line-of-sight column densities and extinctions that exceed the plotted quantities by a factor $\sec \theta$. The presence of multiple clouds on a given sight-line can lead to similar effects.

3.4. Effects of variable fluorine depletion

The theoretical results presented in §3 all assume that the depletion of fluorine nuclei is independent of A_V . The observational data, however, suggest that the fluorine depletion is far greater in dense molecular clouds than in diffuse clouds. In particular, while a gas-phase fluorine abundance $\sim 0.6 \times$ solar has been determined from observations of atomic fluorine in diffuse clouds (see §3.1 above), a gas-phase fluorine abundance of only $\sim 0.02 \times$ solar has been inferred (Neufeld et al. 1998) from far-infrared observations of HF absorption in the dense gas associated with Sgr B2. Similar behavior has been inferred for the element chlorine (Zmuidzinas et al. 1995; Schilke et al. 1995) from submillimeter observations of Sgr B2 and OMC-1.

We have considered the possible effects of fluorine depletion using the simple model described below. A similar model has been recently proposed (Hollenbach et al. 2005) to explain the freeze-out of interstellar oxygen nuclei to form icy grain mantles.

We assume that F atoms and HF molecules in the gas-phase accrete onto dust grains at a rate proportional to the density of dust particles (which, for a fixed gas-to-dust ratio, is proportional to the density of H nuclei, n_{H} .) In the case where F atoms are the accreting

species, we assume that reaction with an adsorbed H atom leads rapidly to the formation that remains bound to the grain mantle⁹. Except for small grains of size $\lesssim 20\text{\AA}$ that are periodically “spike-heated” (Hollenbach et al. 2005) to high temperatures ($\sim 100\text{ K}$), the HF is assumed to remain frozen onto the grain surface until photodesorbed by ultraviolet radiation. Thus we assume HF molecules to be removed by photodesorption via the “direct mechanism” described by Draine and Salpeter (1979), in which excitation of electronic states is followed by ejection from the grain surface with probability, ϵ . Because the ultraviolet photoabsorption cross-section is dominated by photodissociation, the removal rate for F nuclei in the grain mantle is simply given by $\epsilon \zeta_{\text{pd}}(\text{HF})$, where $\zeta_{\text{pd}}(\text{HF})$ is HF photodissociation rate given in Table 4¹⁰. As the HF photodissociation rate drops with increasing extinction, the fraction of fluorine nuclei in the gas-phase diminishes and the abundance of HF ice increases. Our model is motivated by absorption-line observations of water ice (e.g. Whittet et al. 2001), which suggest that significant abundances of water ice are present only in sight-lines along which the extinction exceeds a certain threshold.

In equilibrium, this simple model implies that the ratio of fluorine nuclei in the gas-phase to HF molecules in the solid phase is given by

$$R = \frac{n_{\text{F}}(\text{gas})}{n(\text{solid HF})} = 10^{14} \text{ cm}^{-3} \text{ s} \frac{\epsilon_{-3}}{k_{-17}} \frac{\zeta_{\text{pd}}(\text{HF})}{n_{\text{H}}}, \quad (5)$$

where $10^{-3}\epsilon_{-3}$ is the probability that the electronic excitation of a solid HF molecule will be followed by ejection from the grain mantle, and $10^{-17} k_{-17} n_{\text{H}} \text{ cm}^3 \text{ s}^{-1}$ is the accretion rate per F atom or HF molecule in the gas-phase. Equilibrium is achieved on the accretion timescale, $(3 \text{ Myr}/k_{-17})(10^3/n_{\text{H}})$.

In estimating the ratio ϵ_{-3}/k_{-17} , we turn to the observations of water ice, assuming that the water ice abundance is determined by an analogous balance between photodesorption and accretion. From observations of the $3 \mu\text{m}$ water ice absorption feature in the spectra of a sample of stars in the Taurus region, Whittet et al. (2001) inferred that a threshold extinction $A_V \sim 3.2 \text{ mag}$ was required for a sight-line to yield a significant water ice abundance. Requiring that the quantity $10^{14} (\epsilon_{-3}/k_{-17}) \zeta_{\text{pd}}(\text{H}_2\text{O})/n_{\text{H}}$ should equal unity in a cloud of total extinction $\sim 3.2 \text{ mag}$ (along a diameter), adopting the H_2O photodissociation rate

⁹The probability of retention is unknown, but is probably large (as it is for the grain surface reaction of $\text{O} + \text{H}$, for which a large retention probability $\gtrsim 0.5$ must be invoked to explain the observed abundances of interstellar water ice, e.g. Jones & Williams 1984)

¹⁰Presumably, the ejection probability ϵ drops rapidly with depth below the surface of the grain mantle. Thus, when averaged over all molecules in the mantle, the value of ϵ becomes a decreasing function of mantle thickness once that thickness exceeds a single monolayer.

$\zeta_{\text{pd}}(\text{H}_2\text{O})$ derived by Roberge et al. (1991), and assuming a typical density $n_{\text{H}} \sim 10^3 \text{ cm}^{-3}$ for the clouds probed by the Whittet et al. (2001) study, we obtain an estimate of 0.45 for the ratio (ϵ_{-3}/k_{-17}) . Here we are implicitly assuming that the physics governing the freeze-out of HF is similar to that of H_2O . This assumption seems plausible given the similar dipole moments (both $\sim 1.8 \text{ D}$) and melting points (190 K for HF versus 273 K for H_2O) of HF and H_2 , and the fact that the ultraviolet photoabsorption cross-section is dominated by photodissociation in both cases. We are making an additional approximation by selecting the value of ϵ for the “threshold” extinction and neglecting its variation with grain mantle thickness (see footnote 8).

Given the simple model described above, we may estimate the gas-phase abundance of fluorine nuclei as

$$\frac{n_{\text{F}}(\text{gas})}{n_{\text{H}}} = 1.8 \times 10^{-8} \frac{R}{1 + R} \quad (6)$$

where 1.8×10^{-8} is the “diffuse cloud abundance” ($\sim 0.6 \times \text{solar}$) obtained in the limit of low density and low extinction. Since the timescale for freeze-out is long compared to the timescale for the gas-phase reactions that set the HF/F ratio in the gas, the effect of freeze-out is simply to lower the overall abundances of gas-phase F and HF but to leave their abundance *ratio* unchanged.

We have recomputed the predicted dependence of $N(\text{HF})$ upon $N(\text{H}_2)$, now taking account of variable fluorine depletion with the aid of the equations (5) and (6). The results for a two-sided PDR with $n_{\text{H}} = 10^2$ and $\chi_{UV} = 1$ are represented by the dashed line in Figure 6. As expected, the predicted column densities of gaseous HF are unchanged for small values of $A_V(\text{tot})$, but approach a maximum value at $A_V(\text{tot}) \sim 3$. Results for the parameter study are shown in Figures 9 and 10, which are presented in a manner entirely analogous to Figures 7 and 8.

4. Discussion

The results shown in Figures 2 – 10 show that there is a dramatic tendency towards molecule formation in the chemistry of interstellar fluorine. In diffuse clouds of small extinction, the predicted HF abundance can even exceed that of CO, even though the gas-phase fluorine abundance is four orders of magnitude smaller than that of carbon. In the transition from atomic clouds of small A_V to diffuse molecular clouds, hydrogen and fluorine are the first elements to become molecular. HF is predicted to be the most abundant fluorine-bearing molecule by far; the next most abundant molecule containing fluorine, CF^+ , is expected to show an abundance roughly two orders of magnitude smaller than that of HF. The CF^+/HF

abundance ratio is given by $k_3 n(\text{C}^+)/k_9 n_e$, where k_3 and k_9 are the rate coefficients for reactions R3 (reaction of C^+ with H_2) and R9 (dissociative recombination of CF^+). In the surface layers of the cloud, where the electron and C^+ abundances are nearly equal, the CF^+/HF abundance ratio becomes simply $k_3/k_9 = 0.036(T/300\text{ K})^{0.35}$. In clouds of $A_V \gtrsim 1$ mag, CF^+ column densities $\sim 10^{11}\text{ cm}^{-2}$ are expected. In dense PDRs, with $n_H \gtrsim 10^5\text{ cm}^{-2}$, the CF^+ $J = 1$ and $J = 2$ level populations will approach LTE and face-on brightness temperatures ~ 5 and 20 mK km s^{-1} are expected¹¹ respectively for the $102.6\text{ GHz } J = 1 - 0$ and $205.2\text{ GHz } J = 2 - 1$ transitions. These lines are potentially detectable from ground-based observatories, particularly in nearly edge-on PDRs where the source geometry enhances the brightness of optically-thin lines.

The large predicted abundances for HF provide a strong motivation for future absorption-line observations using airborne or satellite observatories. Such observations are expected to lead to the widespread detection of interstellar HF, even when account is taken of the effects of HF freeze-out (§4.1 above). With its small moment of inertia, HF has a extremely large rotational constant, $B = 20.54\text{ cm}^{-1}$, which places all of its pure rotational transitions at far-infrared wavelengths that are inaccessible to ground-based observatories. To date, observations of interstellar HF have been limited to a single transition in a single source; the $J = 2 - 1$ transition at $121.7\text{ }\mu\text{m}$ was detected by the Infrared Space Observatory (ISO) in absorption towards the source Sgr B2 (NZSP). Because the HF $J = 1 - 0$ transition possesses an extremely large critical density (see §2.3.1 above), significant populations of HF $J = 1$ are typically achieved only in interstellar clouds that are strongly irradiated by far-infrared continuum emission; Sgr B2 is the classic example. The need for strong radiative pumping to populate HF $J = 1$ severely limits the utility of HF $J = 2 - 1$ absorption as a probe of interstellar hydrogen fluoride.

While the HF $J = 1 - 0$ transition at $243.2\text{ }\mu\text{m}$ lies outside the spectral range probed by the ISO spectrometers, it will become observable with the advent of the Stratospheric Observatory for Infrared Astronomy (SOFIA) and the Herschel Space Observatory (HSO). In particular, the CASIMIR instrument on SOFIA and the HIFI instrument on HSO will yield high resolution heterodyne spectroscopy in the relevant spectral region. These instruments will provide an absorption line probe of hydrogen fluoride in its ground rotational state.

Indeed, the HF $J = 1 - 0$ transition promises to yield an extremely sensitive probe of diffuse molecular gas along the line of sight to far-infrared infrared continuum sources. For a cloud with a HF column density $N(\text{HF}) = N_{12} 10^{12}\text{ cm}^{-2}$ and a Doppler parameter

¹¹given a CF^+ dipole moment of 1.04 Debye, the value obtained in the multireference configuration interaction (MRCI) calculations of Peterson et al. (1989)

$b = 10^5 b_5 \text{ cm s}^{-1}$, the line-center optical depth is $\tau_0 = 0.35 N_{12}/b_5$. Thus typical interstellar clouds with HF column densities as small as 10^{12} cm^{-2} should be routinely observable with CASIMIR and HIFI, and HF column densities as small as 10^{11} cm^{-2} are potentially detectable in spectra of high signal-to-noise ratio.

Referring to Figure 6, we find that HF is potentially detectable in diffuse interstellar gas clouds with H_2 column densities smaller than 10^{19} cm^{-2} . To date, the only molecules detected in clouds of such small size are H_2 and HD, observed in absorption toward hot background stars at UV wavelengths¹². This raises the interesting and (at least to us) surprising possibility that spectroscopic observations of far-infrared continuum sources with SOFIA and HSO will reveal a component of foreground molecular gas that is observed primarily by means of its HF absorption lines. Such observations will also be sensitive to HF emission that is intrinsic to the warm, dense background sources themselves.

HF also possesses far-ultraviolet absorption lines that could be searched for in archival stellar spectra obtained with satellite observatories that show diffuse cloud absorption. The most favorable target line is likely the $\text{C}^1\Pi \leftarrow \text{X}^1\Sigma \text{ v} = 0 - 0 \text{ R}(0)$ transition at 951.266\AA (Tashiro et al. 1989) – which has an estimated oscillator strength $f = 0.039$ (Hitchcock et al. 1984) – although very high spectral resolution would be needed to resolve it from the nearby H_2 951.681\AA and NI 951.295\AA features.

Hydrogen fluoride is also a potential probe of molecular material at high redshifts. To date, such material has been studied (1) by means of CO rotational emission lines; and (2) by absorption line spectroscopy of background QSOs at UV/optical and at radio/millimeter wavelengths. Thus far, H_2 has been detected directly at UV and optical wavelengths in 8 damped Lyman alpha systems at redshifts ranging from 2.0 to 3.0, by means of the Lyman and Werner absorption lines (Ledoux, Petitjean, & Srianand 2003), and references therein); the observed molecular fractions, $f = 2N(\text{H}_2)/N_H$, are typically less than 0.03 and the H_2 column densities smaller than $2 \times 10^{18} \text{ cm}^{-2}$. At millimeter wavelengths, foreground molecular gas has been detected in absorption towards 4 high-redshift radio sources at redshifts in the range $z = 0.25 - 0.89$ (Wiklind & Combes 1999; Curran et al. 2004). For absorbing material detected at radio and millimeter wavelengths, the visual extinction along the sight-line is typically large and the molecular fraction is $\sim 0.3 - 1.0$. The list of detected molecules includes CO, HCO^+ , HCN, H_2O , and OH.

¹²HD is also detectable at far-IR wavelengths via its $112\mu\text{m } J = 1 - 0$ transition, which was detected using ISO (Caux et al. 2002) and will be observable using the GREAT instrument on SOFIA. Unfortunately, because the HD dipole moment is so small, the optical depth is only $3 \times 10^{-20} N(\text{HD})/b_5$. Thus, far-IR HD absorption will be detectable only along sight-lines with A_V of at least 10 mag, even in spectra of high signal-to-noise ratio.

HF observations are a potentially valuable bridge between the UV/optical observations capable of probing low column density systems and the radio/millimeter-wavelength observations that probe clouds of high extinction and large molecular fraction. At redshifts beyond $z \sim 0.3$, HF is potentially detectable from ground-based observatories in several atmospheric transmission windows. Because the HF $J = 1 - 0$ rest frequency is considerably higher than that of the CO, HCO⁺, HCN, H₂O, and OH transitions observed to date, and because the continuum fluxes and receiver sensitivities decline with frequency, the large collecting area to be provided by ALMA will likely be needed to make significant progress in high- z observations of HF. In Figure 11, we show the model atmospheric transmission (Pardo, Cernicharo & Serabyn 2001) at the redshifted wavelength of HF $J = 1 - 0$, as a function of the redshift; results apply to the zenith transmission under favorable conditions (0.4 mm precipitable water vapor) at the proposed Chajnantor ALMA site.

We are indebted to C. Zhu for providing us with unpublished rate coefficients for the reaction $F + H_2 \rightarrow HF + H$ over the critical temperature range 10 – 50 K. We are very grateful to the referee for several very helpful comments about the manuscript – and, in particular, for pointing out that CF⁺ may be detectable through ground-based observations at millimeter wavelengths. It is a pleasure also to acknowledge valuable discussions with A. Dalgarno, M. Kaufman, D. Hollenbach, P. Sonnentrucker, P. Dagdigan, and M. Alexander. D.A.N. gratefully acknowledges the support of a grant from NASA’s Long Term Space Astrophysics (LTSA) Research Program. M.G.W. is supported in part by NASA LTSA grant NAG 5-9271.

REFERENCES

- Adams, N. G., Smith, D., and Clary, D. C. 1985, *ApJ*, 296, L31
- Balakrishnan, N. & Dalgarno, A. 2001, *Chem. Phys. Lett.*, 341, 652
- Brown, A., and Balint-Kurti, G. G. 2000, *J. Chem. Phys.* 113, 1870
- Castillo, J. F., Hartke, B., Werner, H.-J., Aoiz, F.J., Banares, L., Martinez-Haya, B. 1998, *J. Chem. Phys.* 109, 7224
- Caux, E., Ceccarelli, C., Pagani, L., Maret, S., Castets, A., & Pardo, J. R. 2002, *A&A*, 383, L9
- Curran, S. J., Murphy, M. T., Pihlström, Y. M., Webb, J. K., Bolatto, A. D., & Bower, G. C. 2004, *MNRAS*, 352, 563

- Dalgarno, A., Yan, M., & Liu, W. 1999, *ApJS*, 125, 237
- Draine, B. T. 1978, *ApJS*, 36, 595
- Federman, S. R., Sheffer, Y., Lambert, D. L., & Smith, V. V. 2005, *ApJ*, 619, 884
- Gredel, R., Lepp, S., Dalgarno, A., & Herbst, E. 1989, *ApJ*, 347, 289
- Habing, H. J. 1968, *Bull. Astron. Inst. Netherlands*, 19, 421
- Hitchcock, A. P., Williams, G. R. J., Brion, C.E., & Langhoff, P. W. 1984, *Chem. Phys.* 88, 65
- Hollenbach, D. J., et al. 2004, in preparation
- Jones, A. P., & Williams, D. A. 1984, *MNRAS*, 209, 955
- Kaufman, M. J., Wolfire, M. G., Hollenbach, D. J., & Luhman, M. L. 1999, *ApJ*, 527, 795 (K99)
- Kaufman, M. J., et al. 2005, in preparation
- Le Bourlot, J., Pineau Des Forets, G., Roueff, E., & Flower, D. R. 1993, *A&A*, 267, 233
- Ledoux, C., Petitjean, P., & Srianand, R. 2003, *MNRAS*, 346, 209
- Le Petit, F., Roueff, E., & Le Bourlot, J. 2002, *A&A*, 390, 369
- LeTeuff, Y. H., Millar, T. J., & Markwick, A. J. 2000, *A&AS*, 146, 157
- Li, A. & Draine, B. T. 2001, *ApJ*, 554, 778
- Mathis, J. S., Mezger, P. G., & Panagia, N. 1983, *A&A*, 128, 212
- McCall, B. J., et al. 2003, *Nature*, 422, 500
- Mezger, P. G., Mathis, J. S., & Panagia, N. 1982, *A&A*, 105, 372
- Nee, J.B., Suto, M., & Lee, L.C. 1985, *J. Phys. B*, 18, 293
- Neufeld, D. A., Zmuidzinas, J., Schilke, P., & Phillips, T. G. 1997, *ApJ*, 488, L141 (NZSP)
- Pardo, J. R., Cernicharo, J., & Serabyn, E. 2001, *IEEE Trans. Ant. and Prop.*, vol. 49, nr. 12
- Parravano, A., Hollenbach, D. J., & McKee, C. F. 2003, *ApJ*, 584, 797

- Péquignot, D. 1990, *A&A*, 231, 499 (Erratum: 313, 1026)
- Peterson, K. A., Woods, R. C., Rosmus, P., Werner, H.-J. 1990, *J. Phys. Chem.*, 93, 1889
- Prasad, S. S., & Tarafdar, S. P. 1983, *ApJ*, 267, 603
- Reese, C., Stoecklin, T., Voronin, A., and Rayez, R. C. 2005, *A&A*, 430, 1139
- Rowe, B. R., Marquette, J. B., Dupeyrat, G., & Ferguson, E. E. 1985, *Chem. Phys. Lett.* 113, 403
- Savage, B. D., Drake, J. F., Budich, W., & Bohlin, R. C. 1977, *ApJ*, 216, 291
- Scott, G. B. I., Fairley, D. A., Freeman, C. G., & McEwan, M. J. 1997, *Chem. Phys. Lett.*, 269, 88
- Snow, T. P. & York, D. G. 1981, *ApJ*, 247, L39
- Stark, K., & Werner, H.-J. 1996, *J. Chem. Phys.* 1996, 104, 6515
- Sternberg, A., Dalgarno, A., & Lepp, S. 1987, *ApJ*, 320, 676
- Stevens, P.S., Brune, W.H., & Anderson, J.G. 1989, *J. Phys. Chem.*, 93, 4068
- Tashiro, L. M., Ubachs, W., & Zare, R. N. 1989, *J. Mol. Spectr.*, 138, 89
- Tielens, A. G. G. M. & Hollenbach, D. 1985, *ApJ*, 291, 722
- Troe, J. 1985, *Chem. Phys. Lett.*, 122, 425
- Troe, J. 1987, *J. Chem. Phys.*, 87, 2773
- Troe, J. 1996, *J. Chem. Phys.*, 105, 6249
- Weingartner, J. C. & Draine, B. T. 2001, *ApJS*, 134, 263
- Wiklind, T. & Combes, F. 1999, *ASP Conf. Ser.* 156: Highly Redshifted Radio Lines, 202
- Wolfire, M. G., Tielens, A. G. G. M., & Hollenbach, D. 1990, *ApJ*, 358, 116
- Wolfire, M. G., McKee, C. F., Hollenbach, D., & Tielens, A. G. G. M. 2003, *ApJ*, 587, 278
- Zhu, C., Krems, R., Dalgarno, A., & Balakrishnan, N. 2002, *ApJ*, 577, 795

Table 1. Enthalpies of formation of hydrides and fluorides¹

Hydrides		Fluorides	
(kJ mol ⁻¹)		(kJ mol ⁻¹)	
HF	-571	CF ⁺	-748
H ₂	-436	SiF ⁺	-608
OH	-428	HF	-571
CH ⁺	-400	SiF	-549
SH	-356	CF	-541
SH ⁺	-350	SF ⁺	-369
CH	-341	SF	-344
SiH ⁺	-315	NF	-303
NH	-314	OF	-220
SiH	-291	F ₂	-159

¹Enthalpies computed relative to the enthalpies of formation of the constituent atoms, using the values recommended by the NIST Chemistry Web book; the tabulated quantity is therefore $\Delta_f H_{\text{gas}}^0(\text{XY}) - \Delta_f H_{\text{gas}}^0(\text{X}) - \Delta_f H_{\text{gas}}^0(\text{Y})$

Table 2. Standard heats of reaction for possible HF-destroying reactions¹

Reaction	Element, X				
	Carbon	Nitrogen	Oxygen	Silicon	Sulfur
$\text{HF} + \text{X} \rightarrow \text{XF} + \text{H}$	30 ²	268	351	21	227
$\text{HF} + \text{X}^+ \rightarrow \text{XF}^+ + \text{H}$	-178 ³	33	269	-38	202
$\text{HF} + \text{XH} \rightarrow \text{XF} + \text{H}_2$	-66	146	343	-123	147
$\text{HF} + \text{XH}^+ \rightarrow \text{XF}^+ + \text{H}_2$	-213	30	319	-159	116

¹Values computed using the enthalpies of formation recommended by the NIST Chemistry Web book. For ion-neutral reactions, the ionization potentials recommended by the NIST Chemistry Web book were adopted, and any differences between the specific heat capacity of each ion and its corresponding neutral were neglected.

²In units of kJ mol^{-1}

³Exothermic reactions are flagged by boldface type

Table 3. Proton affinities

<hr/> <hr/>	
(kJ mol ⁻¹)	
<hr/>	
F	340
H ₂	422
HF	484
N ₂	494
CO	594
H ₂ O	691

Table 4. Reaction list for F-bearing species

Reaction	Rate/rate coefficient
$F + H_2 \rightarrow HF + H$	$1.0 \times 10^{-10} [\exp(-450 \text{ K}/T) + 0.078 \exp(-80 \text{ K}/T) + 0.0155 \exp(-10 \text{ K}/T)] \text{ cm}^3 \text{ s}^{-1}$
$F + H_2O \rightarrow HF + OH$	$1.6 \times 10^{-10} \text{ cm}^3 \text{ s}^{-1}$
$C^+ + HF \rightarrow CF^+ + H$	$7.2 \times 10^{-9} (T/300 \text{ K})^{-0.15} \text{ cm}^3 \text{ s}^{-1}$
$Si^+ + HF \rightarrow SiF^+ + H$	$5.7 \times 10^{-9} (T/300 \text{ K})^{-0.15} \text{ cm}^3 \text{ s}^{-1}$
$H_3^+ + HF \rightarrow H_2 + H_2F^+$	$1.2 \times 10^{-8} (T/300 \text{ K})^{-0.15} \text{ cm}^3 \text{ s}^{-1}$
$He^+ + HF \rightarrow H + F^+ + He$	$1.1 \times 10^{-8} (T/300 \text{ K})^{-0.15} \text{ cm}^3 \text{ s}^{-1}$
$F^+ + H_2 \rightarrow HF^+ + H$	$1.0 \times 10^{-9} \text{ cm}^3 \text{ s}^{-1}$
$HF^+ + H_2 \rightarrow H_2F^+ + H$	$1.3 \times 10^{-9} \text{ cm}^3 \text{ s}^{-1}$
$CF^+ + e \rightarrow C + F$	$2.0 \times 10^{-7} (T/300 \text{ K})^{-0.5} \text{ cm}^3 \text{ s}^{-1}$
$SiF^+ + e \rightarrow Si + F$	$2.0 \times 10^{-7} (T/300 \text{ K})^{-0.5} \text{ cm}^3 \text{ s}^{-1}$
$HF^+ + e \rightarrow H + F$	$2.0 \times 10^{-7} (T/300 \text{ K})^{-0.5} \text{ cm}^3 \text{ s}^{-1}$
$H_2F^+ + e \rightarrow HF + H$	$3.5 \times 10^{-7} (T/300 \text{ K})^{-0.5} \text{ cm}^3 \text{ s}^{-1}$
$H_2F^+ + e \rightarrow F + \text{products}$	$3.5 \times 10^{-7} (T/300 \text{ K})^{-0.5} \text{ cm}^3 \text{ s}^{-1}$
$F + CH \rightarrow HF + C$	$1.6 \times 10^{-10} \text{ cm}^3 \text{ s}^{-1}$
$F + OH \rightarrow HF + O$	$1.6 \times 10^{-10} \text{ cm}^3 \text{ s}^{-1}$
$F + H_3^+ \rightarrow H_2F^+ + H$	$4.8 \times 10^{-10} \text{ cm}^3 \text{ s}^{-1}$
$HF + h\nu \rightarrow H + F$	$1.17 \times 10^{-10} \chi_{UV} [\frac{1}{2} E_2(2.21 A_V) + \frac{1}{2} E_2(2.21 [A_{V,\text{tot}} - A_V])] \text{ s}^{-1} + 87 \zeta_{cr} / (1 - \omega)$

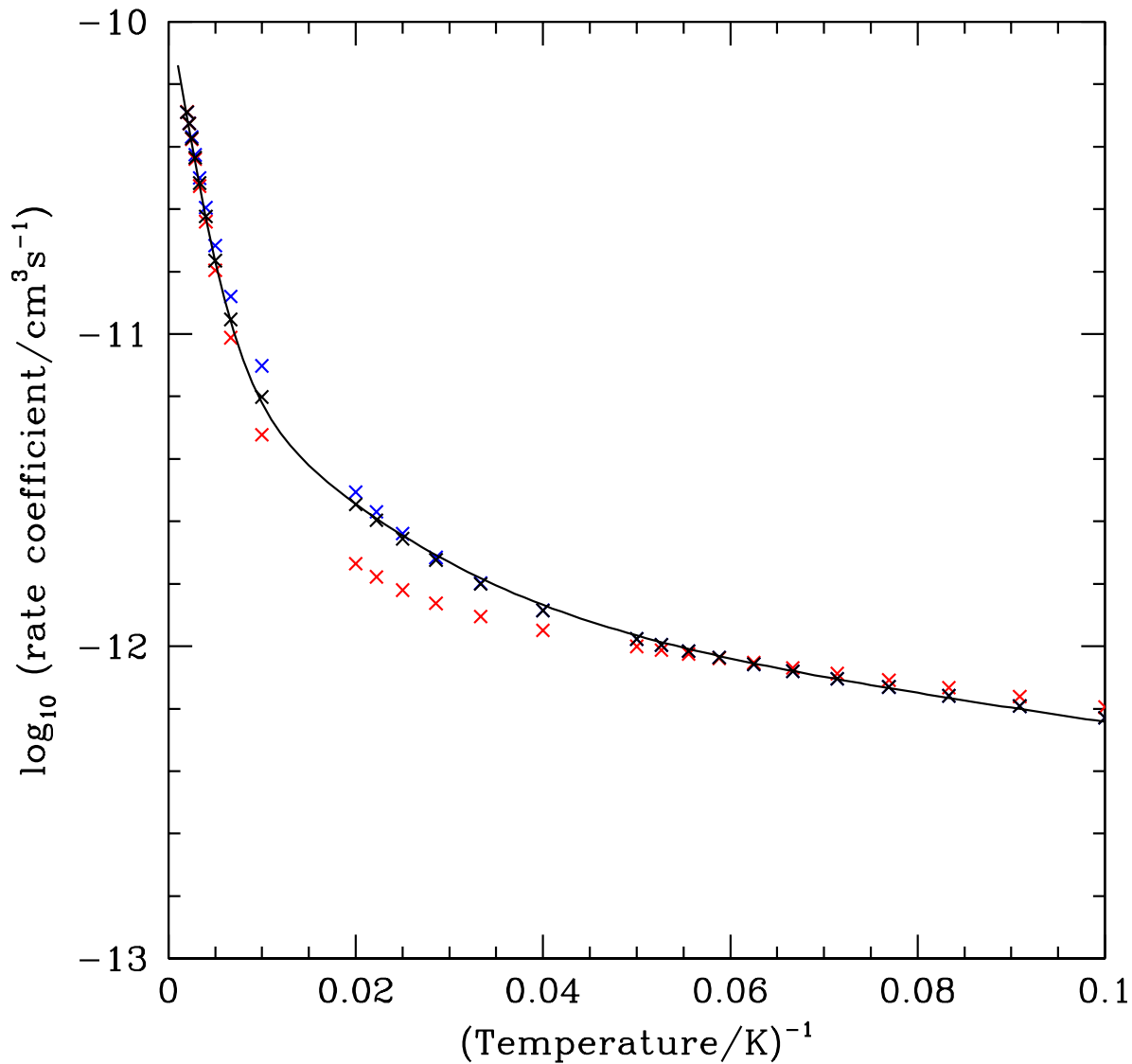


Fig. 1.— Rate coefficients computed by Zhu et al. for the reaction of F ($^2P_{3/2}$) with H₂ $J = 0$ (red crosses) and $J = 1$ (blue crosses). Black crosses show a weighted average applicable when the H₂ populations are in local thermodynamic equilibrium, and the solid black curve shows our adopted fit to that average (see Table 4), which is accurate to better than 5% throughout the temperature range plotted.

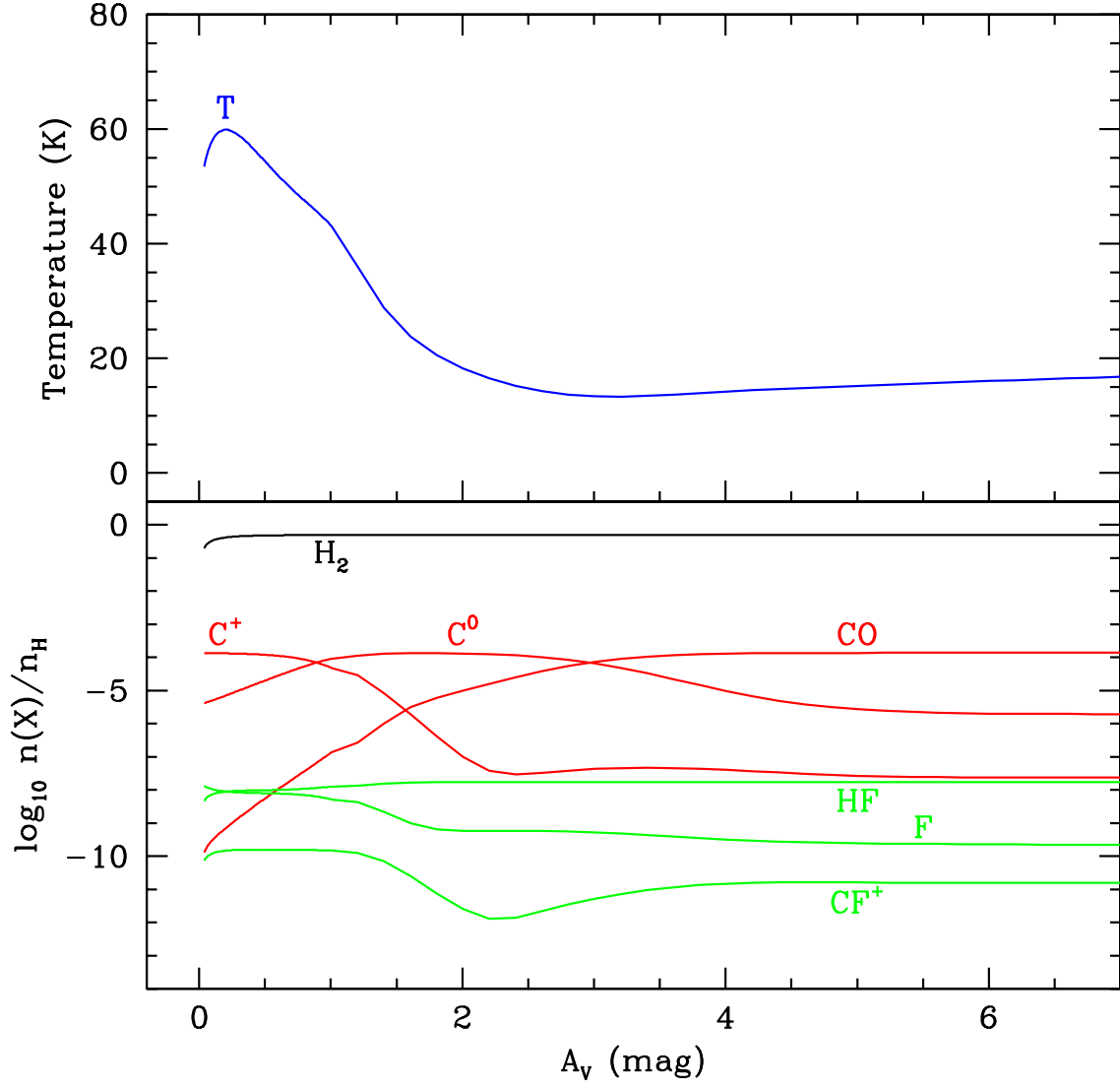


Fig. 2.— Gas temperature and abundances in a one-sided PDR with $n_H = 10^2 \text{ cm}^{-3}$ and $\chi_{UV} = 1$.

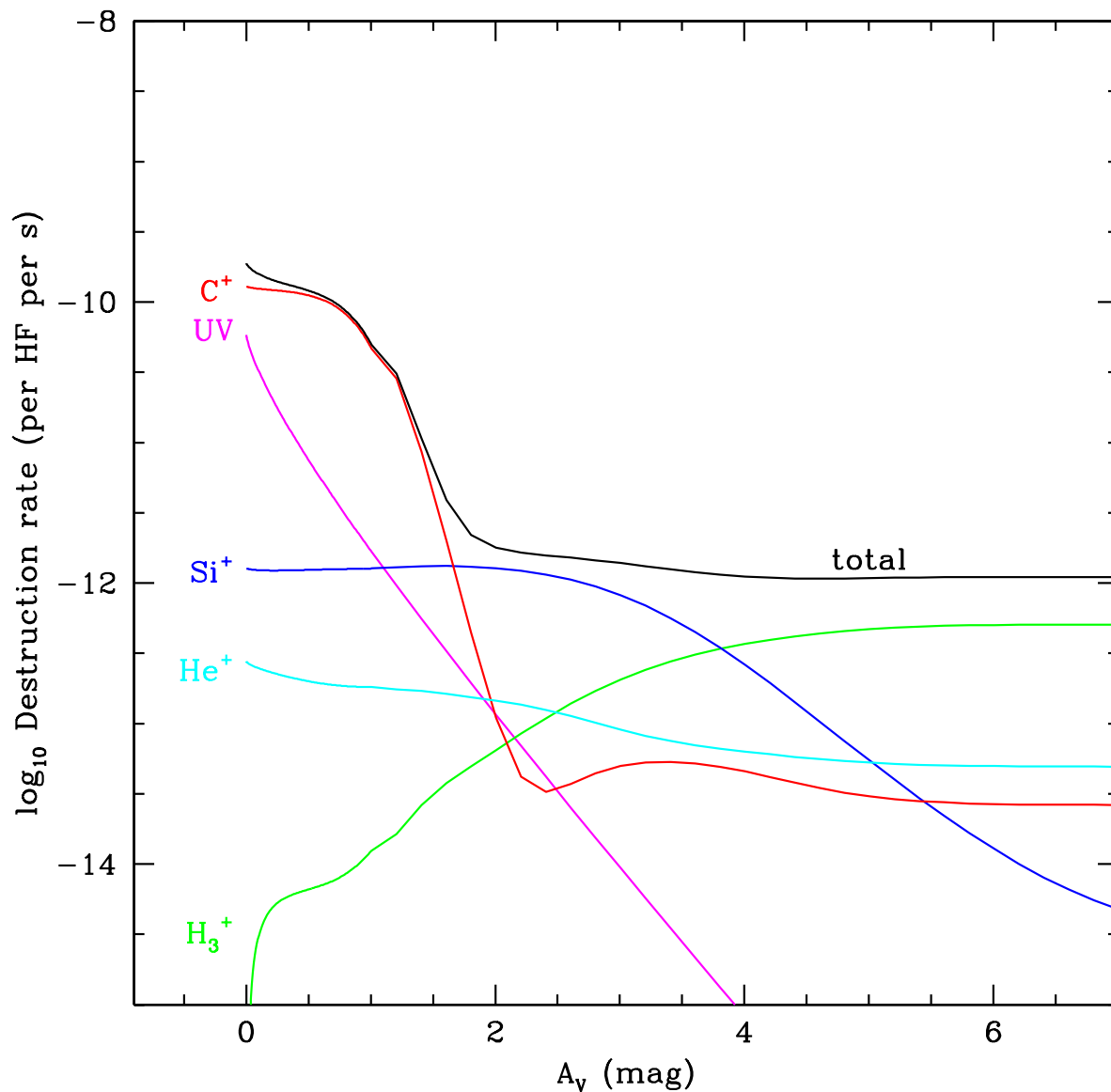


Fig. 3.— HF destruction rates in a one-sided PDR with $n_H = 10^2 \text{ cm}^{-3}$, $\chi_{UV} = 1$. Destruction rates are shown for photodissociation by ISUV (magenta curve) and for reactions with C^+ (red), Si^+ (blue), He^+ (cyan) and H_3^+ (green). The black curve shows the total HF destruction rate.

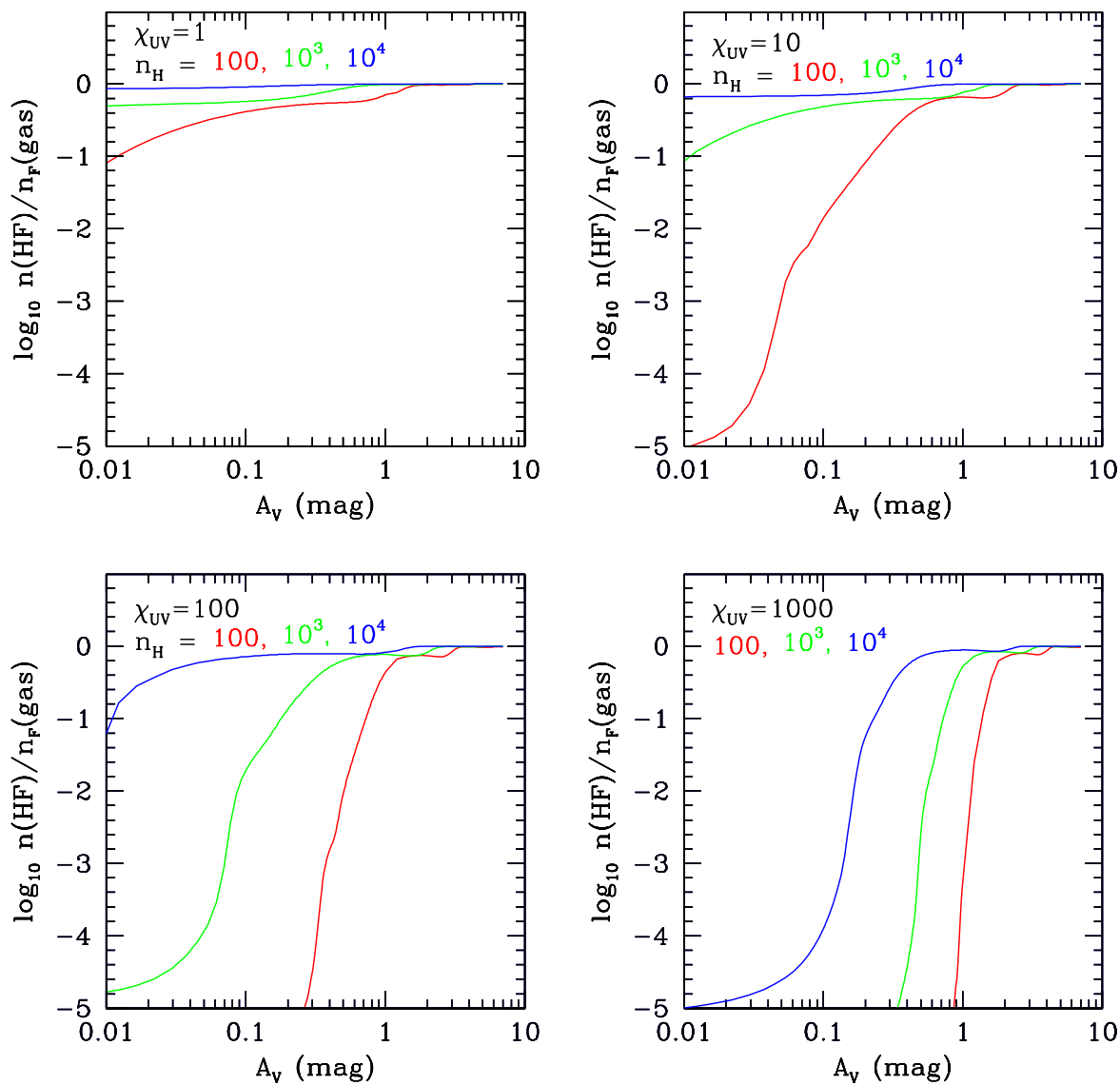


Fig. 4.— HF abundance profiles, $n(\text{HF})/n_{\text{F}}(\text{gas})$, for one-sided PDRs with $n_{\text{H}} = 10^2, 10^3$, and 10^4 cm^{-3} irradiated by ISUV fields of $\chi_{\text{UV}} = 1, 10, 100$, and 1000.

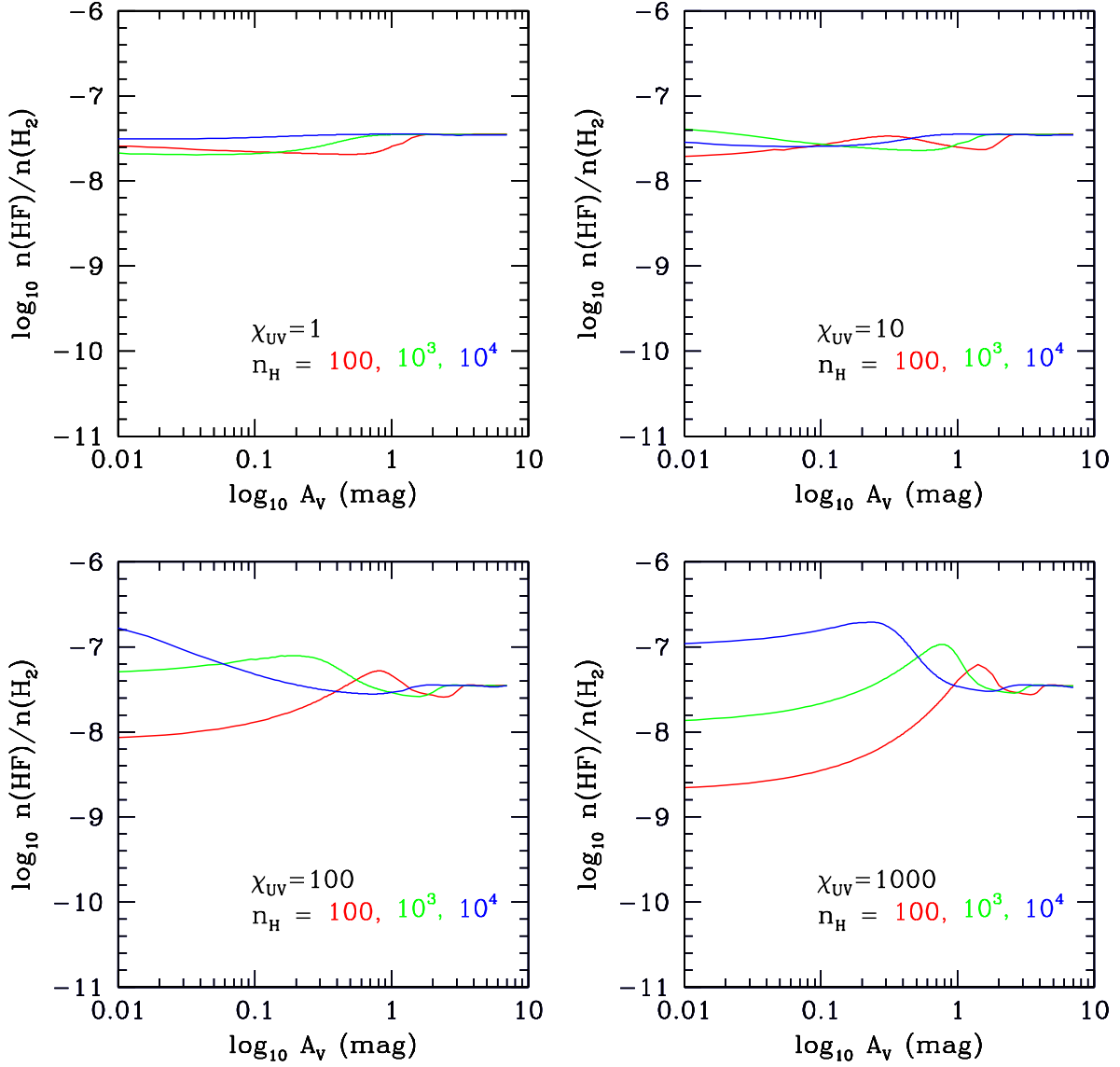


Fig. 5.— HF abundance profiles, $n(\text{HF})/n\text{H}_2$, for one-sided PDRs with $n_{\text{H}} = 10^2, 10^3$, and 10^4 cm^{-3} irradiated by ISUV fields of $\chi_{\text{UV}} = 1, 10, 100$, and 1000 . (Same as Fig. 4, but now with the HF abundance expressed relative to H₂ instead of gas-phase fluorine nuclei.)

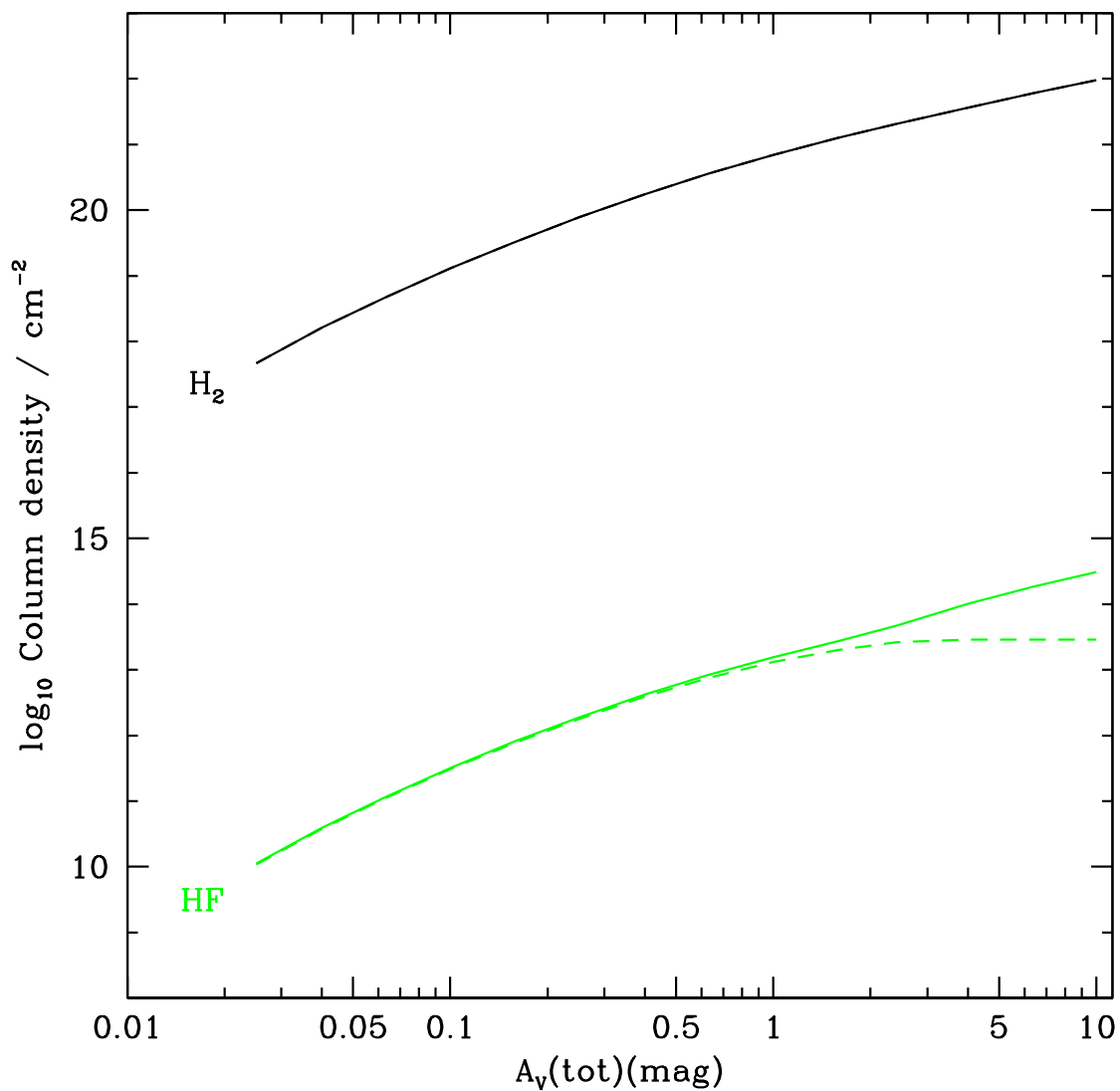


Fig. 6.— HF and H_2 column densities, for a two-sided PDR with $n_{\text{H}} = 10^2$ and $\chi_{UV} = 1$. Results are plotted as a function of total visual extinction through the cloud, $A_V(\text{tot})$. Solid curves: results for fixed fluorine depletion; dashed curve: results for variable fluorine depletion (i.e. with freeze-out included; see §3.4)

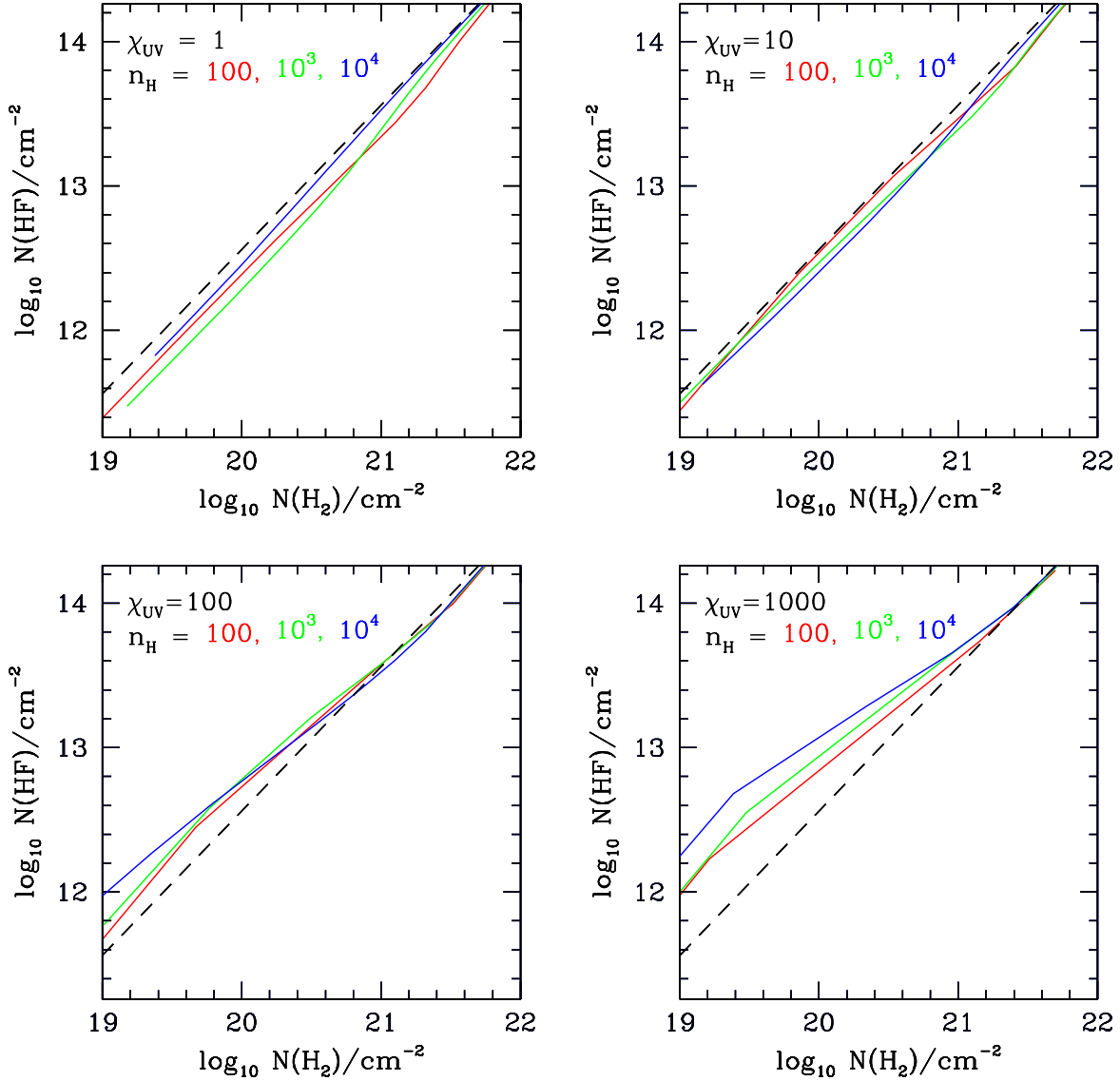


Fig. 7.— HF column densities versus H_2 column density, for two-sided PDRs with $n_{\text{H}} = 10^2$, 10^3 , and 10^4 cm^{-3} irradiated by ISUV fields of $\chi_{\text{UV}} = 1, 10, 100$, and 1000 . The dashed line corresponds to $N(\text{HF})/N(\text{H}_2) = 3.6 \times 10^{-8}$, the value obtained in the limit where H_2 and HF are the sole gas-phase reservoirs of H and F nuclei. Results are presented for fixed fluorine depletion.

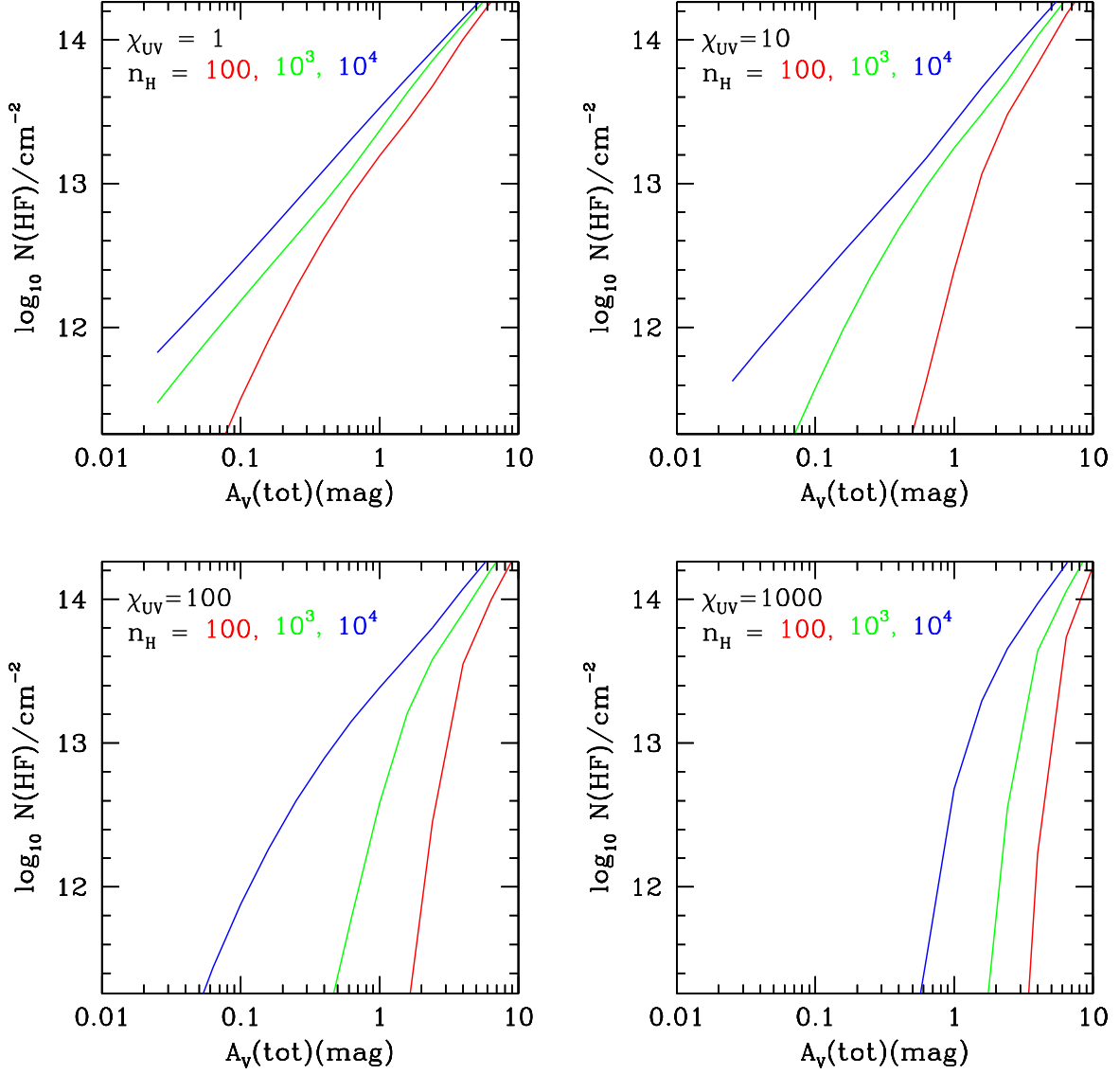


Fig. 8.— HF column densities versus total visual extinction, for two-sided PDRs with $n_{\text{H}} = 10^2, 10^3$, and 10^4 cm^{-3} irradiated by ISUV fields of $\chi_{\text{UV}} = 1, 10, 100$, and 1000 . Results are presented for fixed fluorine depletion.

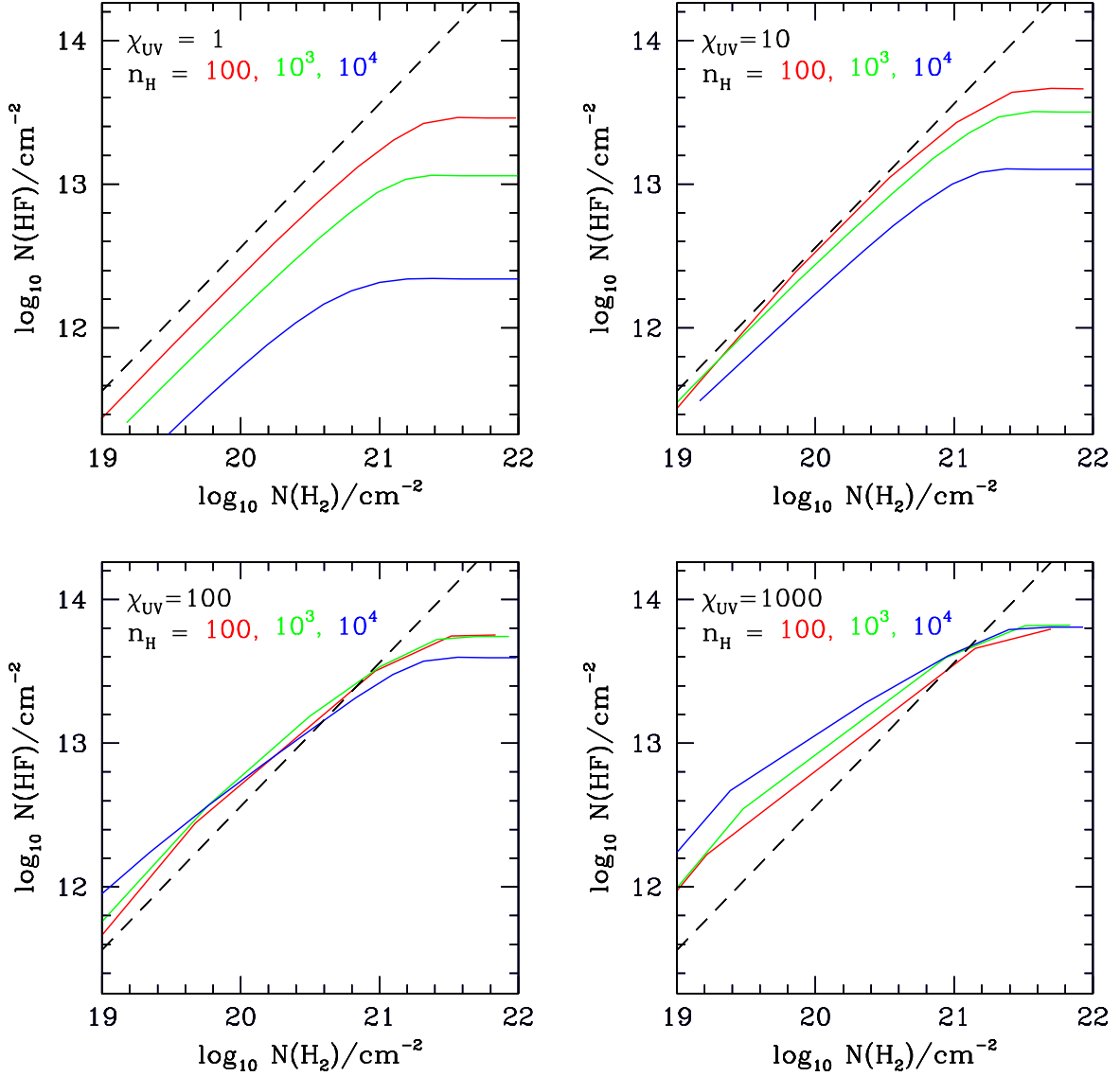


Fig. 9.— HF column densities versus H₂ column density, for two-sided PDRs with $n_{\text{H}} = 10^2$, 10^3 , and 10^4 cm^{-3} irradiated by ISUV fields of $\chi_{\text{UV}} = 1, 10, 100$, and 1000 . The dashed line corresponds to $N(\text{HF})/N(\text{H}_2) = 3.6 \times 10^{-8}$, the value obtained in the limit where H₂ and HF are the sole gas-phase reservoirs of H and F nuclei. Results are presented for variable fluorine depletion (i.e. with freeze-out included; see §3.4)

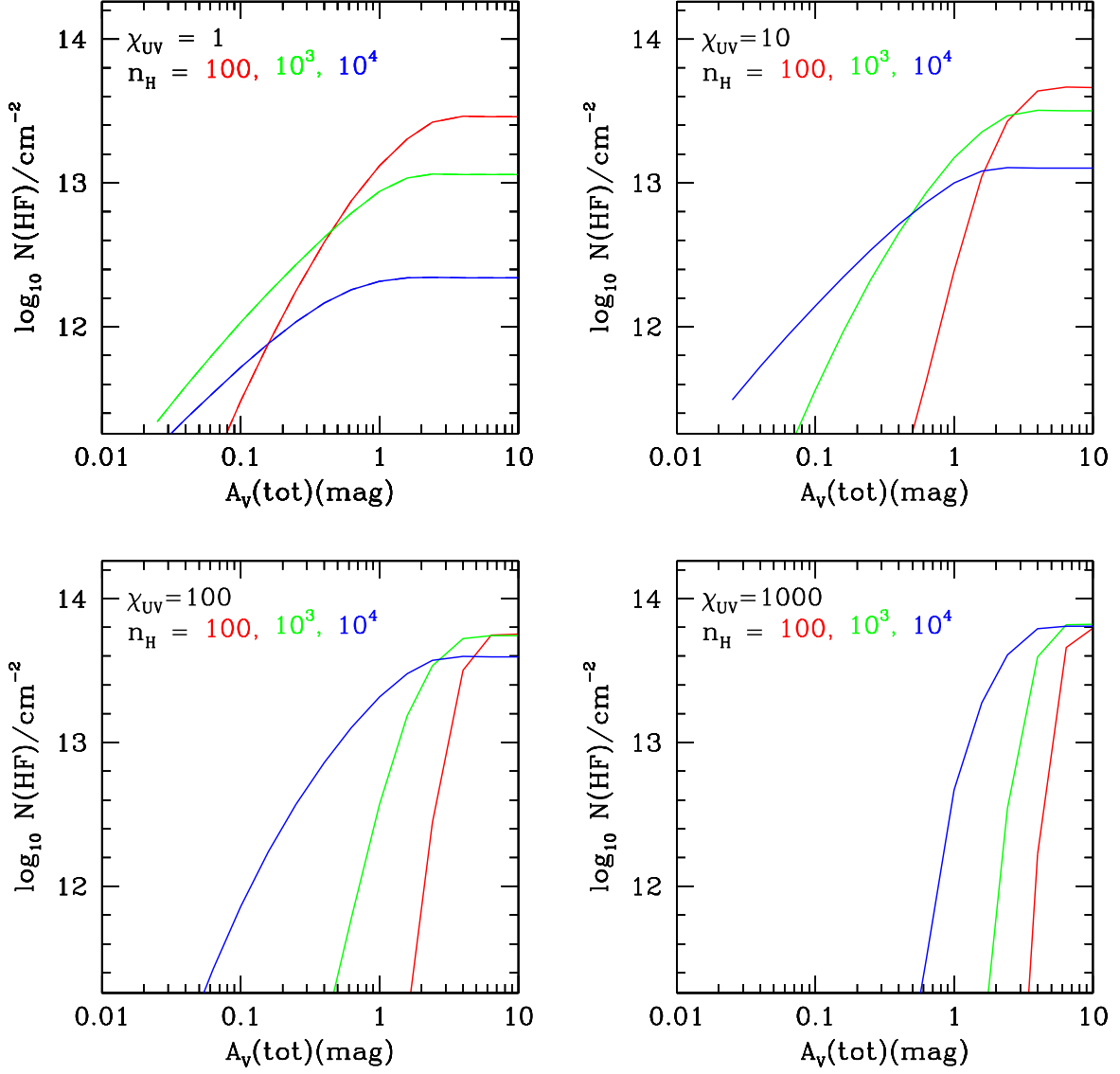


Fig. 10.— HF column densities versus total visual extinction, for two-sided PDRs with $n_H = 10^2, 10^3$, and 10^4 cm^{-3} irradiated by ISUV fields of $\chi_{UV} = 1, 10, 100$, and 1000. Results are presented for variable fluorine depletion (i.e. with freeze-out included; see §3.4)

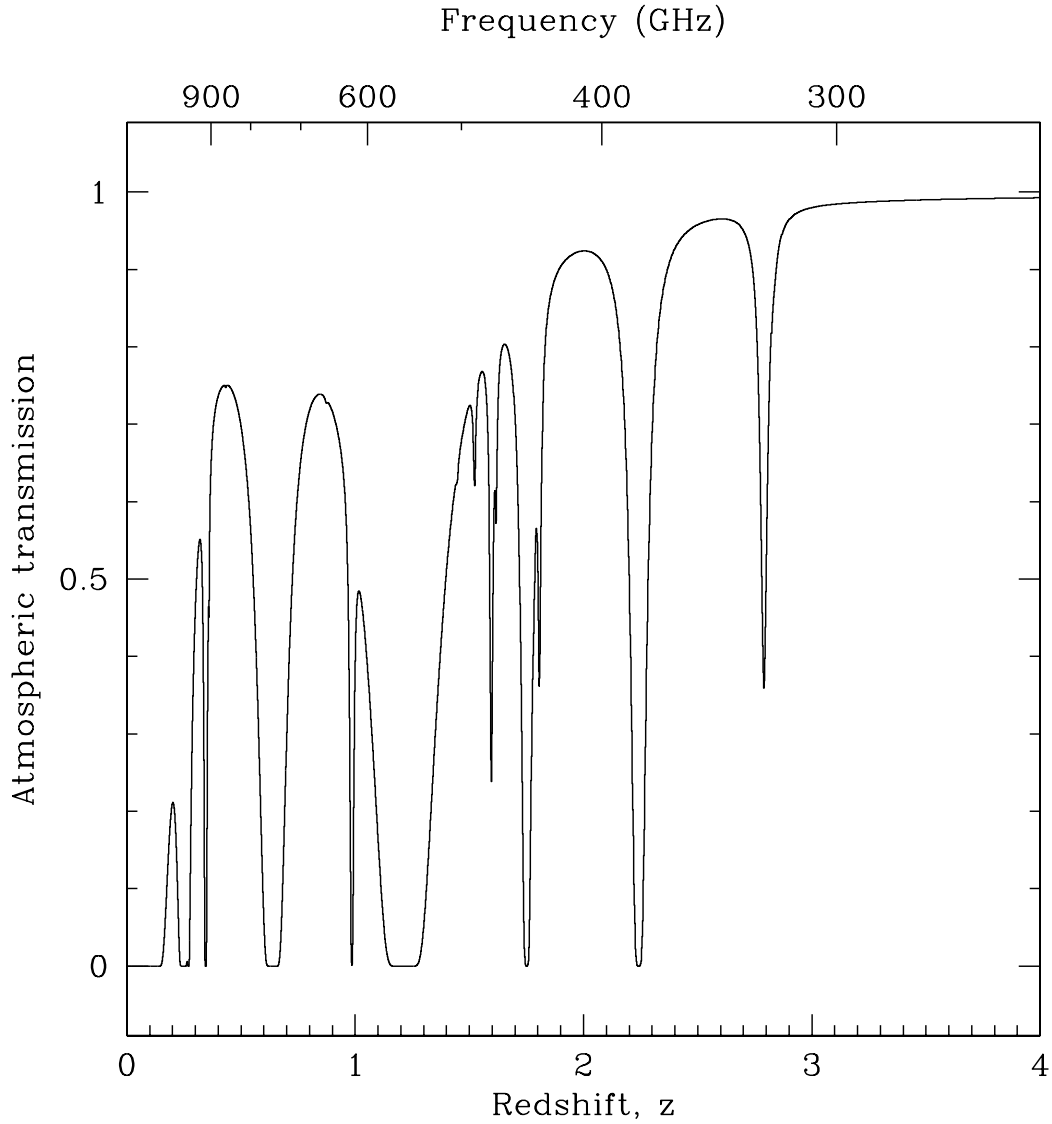


Fig. 11.— Model atmospheric transmission (Pardo, Cernicharo & Serabyn 2001) at the redshifted wavelength of HF $J = 1 - 0$, as a function of the redshift; results apply to the zenith transmission under favorable conditions (0.4 mm precipitable water vapor) at the proposed Chajnantor ALMA site. The line rest frequency is 1232.476 GHz